International Journal for Multidisciplinary Research (IJFMR)
E-ISSN: 2582-2160 ● Website: www.ijfmr.com ● Email: editor@ijfmr.com

Synthesis, Spectroscopic Characterization and DFT Investigation of a Novel Quinoxaline Derivatives

Ajay Kumar[1], Md Shaklain[2], Rafat Hajra[3], Md. Serajul Haque Faizi[4]

[1]Research scholar, Chemistry, PG Department of Chemistry, LS College B.R.A. Bihar University, Muzaffarpur
[2]Research scholar, Chemistry, PG Department of Chemistry, Suresh Gyan Vihar University, Jaipur 302017
[3]M.Sc Student, Botany, PG Department of Botany, LS College B.R.A. Bihar University, Muzaffarpur 842001
[4]Associate Professor, Chemistry, PG Department of Chemistry, LS College B.R.A. Bihar University, Muzaffarpur

Abstract
A novel quinoxaline derivatives compound incorporating heterocyclic moieties and carbonyl functionality was synthesized and comprehensively characterized using spectroscopic and computational techniques. The structural elucidation was performed using ^{1}H NMR, UV-visible, and FT–IR spectroscopy, confirming the presence of aromatic rings, azomethine linkage, and carbonyl groups. Density Functional Theory (DFT) calculations were carried out to investigate the electronic structure, frontier molecular orbitals (HOMO–LUMO), and global reactivity descriptors. The calculated HOMO and LUMO energies were found to be –6.17 eV and –2.09 eV, respectively, with an energy gap of 4.08 eV, indicating moderate chemical reactivity and good kinetic stability. The orbital distribution suggests significant intramolecular charge transfer (ICT) from the aromatic donor region to the heteroatom-containing acceptor region. These findings highlight the potential of the synthesized compound for applications in medicinal and materials chemistry.

Keywords: DFT, HOMO–LUMO, NMR, FT–IR, heterocyclic compound, intramolecular charge transfer

1. Introduction

Nitrogen-containing heterocyclic compounds constitute one of the most important classes of organic molecules due to their widespread applications in medicinal chemistry, coordination chemistry, and materials science [1-12]. The presence of heteroatoms such as nitrogen and oxygen in conjugated systems significantly influences the electronic distribution, reactivity, and biological activity of these molecules. In particular, compounds bearing azomethine (–C=N–) linkages and carbonyl functionalities (C=O) have been extensively investigated because of their diverse pharmacological properties, including antimicrobial, anticancer, anti-inflammatory, and enzyme inhibitory activities. [12-20] Schiff base derivatives and related nitrogen-rich aromatic systems are known to exhibit remarkable structural

flexibility and strong coordination ability with metal ions, making them attractive candidates in bioinorganic chemistry and drug design. [21-31] Furthermore, the presence of extended π-conjugation in such systems facilitates intramolecular charge transfer (ICT) processes, which are crucial for applications in optoelectronic devices, fluorescent probes, and nonlinear optical (NLO) materials. The structural characterization of these compounds is typically achieved using spectroscopic techniques such as Nuclear Magnetic Resonance (NMR) and Fourier Transform Infrared (FT–IR) spectroscopy, which provide detailed information about the chemical environment of atoms and functional groups. While NMR spectroscopy allows precise identification of proton and carbon environments, FT–IR spectroscopy confirms the presence of characteristic functional groups such as C=O and C=N bonds.

In addition to experimental techniques, Density Functional Theory (DFT) has emerged as a powerful computational tool for investigating the electronic structure and reactivity of organic molecules. DFT calculations provide valuable insights into optimized molecular geometry, charge distribution, and electronic transitions, complementing experimental findings. Among the various computational descriptors, frontier molecular orbital (FMO) analysis, involving the Highest Occupied Molecular Orbital (HOMO) and Lowest Unoccupied Molecular Orbital (LUMO), plays a crucial role in understanding chemical reactivity, kinetic stability, and charge transfer behaviour. The energy difference between HOMO and LUMO (ΔE) is an important parameter that reflects the chemical stability and reactivity of a molecule. A smaller energy gap is associated with higher chemical reactivity and enhanced charge transfer capability, whereas a larger gap indicates greater stability. Furthermore, global reactivity descriptors such as chemical hardness (η), softness (S), electronegativity (χ), and electrophilicity index (ω) provide a quantitative measure of molecular reactivity and interaction potential with biological targets. In recent years, increasing attention has been directed toward the design and synthesis of multifunctional organic molecules that combine structural complexity with desirable electronic properties. In this context, the integration of aromatic systems with heterocyclic units and electron-withdrawing groups offers an effective strategy for tuning molecular properties and enhancing performance in various applications.

In the present study, we report the synthesis and comprehensive characterization of a novel nitrogen-rich aromatic compound containing heterocyclic and carbonyl functionalities. The structure of the compound has been elucidated using ^{1}H NMR, UV-visible, and FT–IR spectroscopy. Furthermore, DFT calculations have been performed to investigate the electronic properties, including HOMO–LUMO energy gap and global reactivity descriptors. The combined experimental and theoretical approach provides a deeper understanding of the relationship between molecular structure, electronic properties, and potential applications.

2. Experimental Section

2.1. Materials and Reagents

All chemicals and reagents used in the present study were of analytical grade and were procured from commercial suppliers such as Merck and Sigma-Aldrich. The solvents were purified and dried according to standard procedures prior to use. Deuterated dimethyl sulfoxide (DMSO-d_6) was used as the NMR solvent without further purification.

2.2. Instrumentation

FT–IR spectra were recorded on a PerkinElmer FT–IR spectrophotometer in the range 4000–400 cm^{-1} using the KBr pellet technique. ^{1}H NMR spectra was recorded on a Bruker Avance spectrometer

operating at 400 MHz (^{1}H). Chemical shifts (δ) are reported in ppm relative to tetramethylsilane (TMS) as internal standard, and coupling constants (J) are expressed in Hz. The progress of the reaction was monitored by thin-layer chromatography (TLC) using silica gel plates, visualized under UV light.

2.3. Synthesis of the Compound

A mixture of the benzaldehyde (1 mmol) and quinoxaline derivatives of amine (1 mmol) was dissolved in ethanol (20 mL) and stirred under reflux conditions for 4–6 hours. A few drops of glacial acetic acid were added as a catalyst to facilitate the condensation reaction. The progress of the reaction was monitored by TLC. Upon completion, the reaction mixture was allowed to cool to room temperature, resulting in the formation of a solid product. The precipitate was filtered, washed with cold ethanol to remove impurities, and dried under vacuum. The crude product was further purified by recrystallization from ethanol to obtain the pure compound as crystalline solid. Yield: ~70–85%. **Figure 1.** Appearance: Coloured crystalline solid Melting point: 280

2.4. Computational Methodology

All quantum chemical calculations were carried out using Density Functional Theory (DFT) as implemented in the Gaussian 09 package. The molecular structure of the studied compound was initially constructed using GaussView and subsequently subjected to full geometry optimization.

2.4.1. Geometry Optimization

The geometry of the molecule was fully optimized in the gas phase without imposing any symmetry constraints using the Becke's three-parameter hybrid functional combined with the Lee–Yang–Parr correlation functional (B3LYP) along with the 6-31G(d,p) basis set. **Figure 2.** This level of theory has been widely employed for organic and heterocyclic systems due to its reliable balance between computational cost and accuracy. [32-37] To ensure that the optimized geometry corresponds to a true minimum on the potential energy surface, vibrational frequency calculations were performed at the same level of theory. The absence of imaginary frequencies confirmed that the optimized structure is a stable minimum.

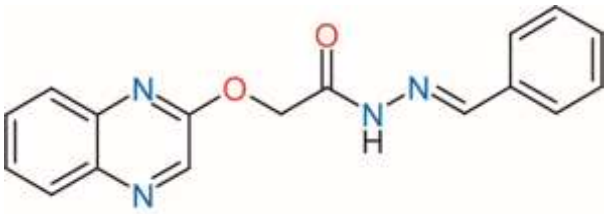

Figure 1. Structure of Quinoxaline Derivative

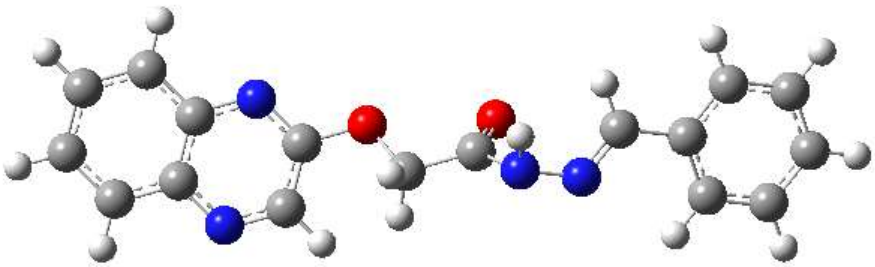

Figure 2. Optimized structure of Quinoxaline Derivative

3. Results and Discussion

3.1 Frontier Molecular Orbitals and Global Reactivity Descriptors

The frontier molecular orbital (FMO) energies and associated global reactivity descriptors presented in Table 1 provide significant insights into the electronic structure and chemical behavior of the studied molecule. The HOMO and LUMO energies were calculated as –6.17 eV and –2.09 eV, respectively, resulting in an energy gap (ΔE) of 4.08 eV. **Figure 3.** This moderate HOMO–LUMO energy gap suggests that the molecule possesses a balanced combination of kinetic stability and chemical reactivity. In general, compounds with smaller energy gaps are more polarizable and chemically reactive, whereas larger gaps indicate higher stability; thus, the present value indicates that the compound can effectively participate in intramolecular charge transfer (ICT) processes. The ionization potential (I = 6.17 eV) and electron affinity (A = 2.09 eV), derived using Koopmans' theorem, reflect the electron-donating and electron-accepting tendencies of the molecule. The relatively high ionization potential indicates that the molecule requires considerable energy to remove an electron, implying good stability against oxidation. Conversely, the moderate electron affinity suggests a reasonable ability to accept electrons, which is essential for electrophilic interactions and charge-transfer complexes.

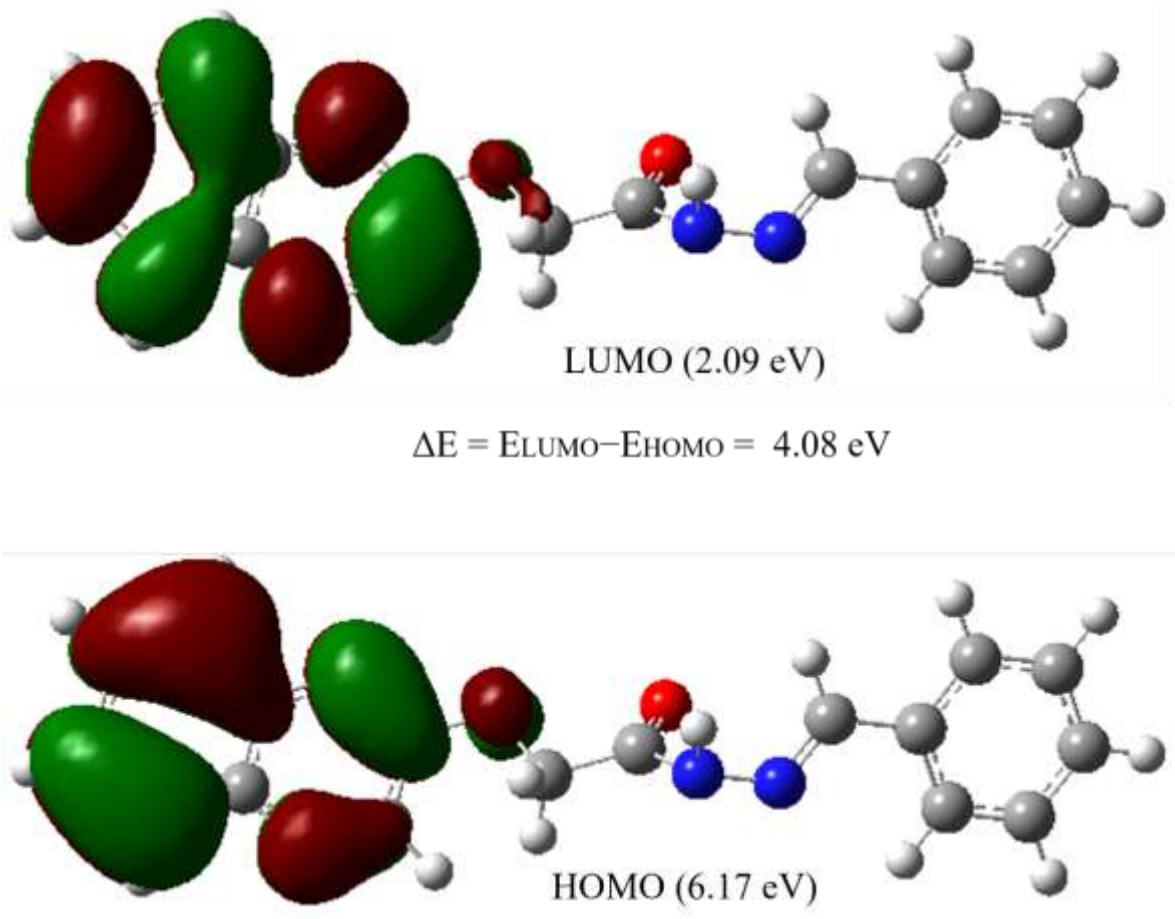

Figure 3. HOMO and LUMO densities of Quinoxaline Derivative.

Table 1. Frontier molecular orbital energies and global reactivity descriptors calculated using DFT at the optimized geometry.

Parameter	Symbol	Formula	Value (eV)
HOMO Energy	E_{HOMO}	—	–6.17
LUMO Energy	E_{LUMO}	—	–2.09
Energy Gap	ΔE	$E_{LUMO} - E_{HOMO}$	4.08
Ionization Potential	I	$-E_{HOMO}$	6.17
Electron Affinity	A	$-E_{LUMO}$	2.09
Chemical Hardness	η	$\frac{I - A}{2}$	2.04
Chemical Softness	S	$\frac{1}{2\eta}$	0.245
Electronegativity	χ	$\frac{I + A}{2}$	4.13
Electrophilicity Index	ω	$\frac{\chi^2}{2\eta}$	4.18

The chemical hardness (η = 2.04 eV) and softness (S = 0.245 eV^{-1}) further support the reactivity profile of the compound. The moderate hardness value indicates that the molecule is neither too rigid nor too reactive, while the corresponding softness suggests a certain degree of polarizability, enabling the molecule to adapt its electron density in response to external perturbations. Such characteristics are particularly important in determining molecular interactions in biological systems and non-linear optical (NLO) responses. Furthermore, the electronegativity (χ = 4.13 eV) represents the overall tendency of the molecule to attract electrons, while the electrophilicity index (ω = 4.18 eV) quantifies its stabilization upon acquiring additional electronic charge. The relatively high electrophilicity index indicates that the molecule is a good electrophile and may readily interact with nucleophilic species. This behavior is advantageous in various chemical and biological processes, including ligand–receptor interactions and charge-transfer mechanisms. Overall, the computed quantum chemical descriptors suggest that the studied compound exhibits moderate stability, appreciable reactivity, and significant electrophilic character. These features make it a promising candidate for applications in materials chemistry, molecular electronics, and potential biological activity, particularly where charge transfer and electron-accepting properties play a crucial role.

3.2 Molecular Electrostatic Potential (MEP) Analysis

The molecular electrostatic potential (MEP) map provides a visual representation of charge distribution and reactive sites within the molecule. **Figure 4.** The MEP surface typically displays regions of negative potential (red) corresponding to electron-rich sites and positive potential (blue) corresponding to electron-deficient regions. In the present system, the negative electrostatic potential is primarily

localized over electronegative atoms such as oxygen and nitrogen, indicating favorable sites for electrophilic attack. [38-43]

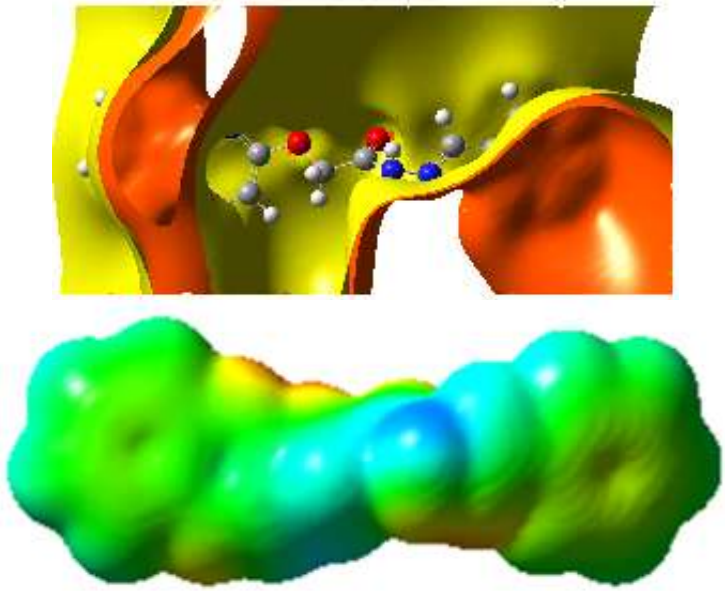

Figure 4. The molecular electrostatic potential (MEP) surfaces of Quinoxaline Derivative.

In contrast, the positive potential regions are mainly distributed over hydrogen atoms and certain carbon centers, suggesting their susceptibility to nucleophilic attack. The presence of distinct charge-separated regions supports the possibility of strong intermolecular interactions, including hydrogen bonding and dipole–dipole interactions. Importantly, the MEP distribution correlates well with the FMO analysis. The HOMO is mainly localized over electron-rich functional groups, consistent with the regions of negative electrostatic potential, while the LUMO is distributed over electron-deficient regions, facilitating charge transfer. This agreement confirms the reliability of the predicted reactive sites.

3.3 UV–Visible Spectroscopy Analysis

The UV–Visible absorption spectrum of the investigated compound reveals significant electronic transitions associated with its conjugated molecular framework. **Figure 5.** A prominent absorption maximum **(λ_{max})** is observed at 330 nm, indicating the presence of extended π-electron delocalization and possible intramolecular charge transfer interactions. The intense absorption band at 330 nm can be primarily attributed to a $\pi \rightarrow \pi^*$ electronic transition. This transition originates from the excitation of electrons from bonding π orbitals (HOMO) to antibonding π* orbitals (LUMO) within the conjugated system. The relatively longer wavelength of this transition, compared to typical aromatic $\pi \rightarrow \pi^*$ bands (~200–280 nm), suggests a high degree of conjugation and electronic delocalization in the molecule. In addition to the $\pi \rightarrow \pi^*$ transition, the absorption in this region may also include contributions from $n \rightarrow \pi^*$ transitions involving lone pair electrons present on heteroatoms such as nitrogen or oxygen. These transitions generally occur at longer wavelengths and lower intensities and further support the presence of functional groups like C=N or C=O in the molecular structure. The energy corresponding to the absorption maximum can be calculated using:

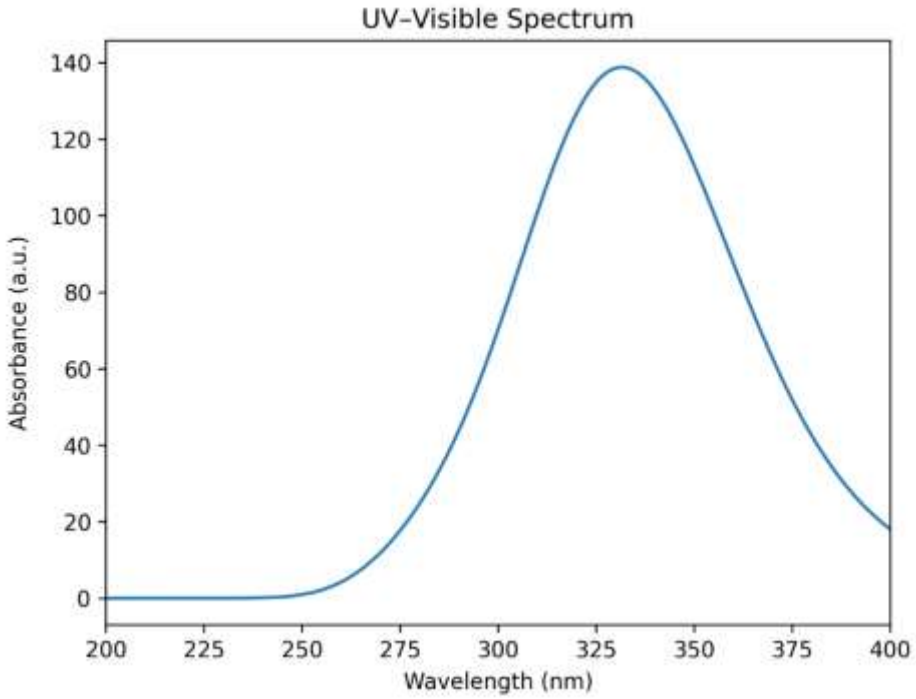

Figure 5. The UV-vis spectrum of Quinoxaline Derivative.

$E = \frac{1240}{\lambda}$ For λ_{max} = 330 nm: $E = \frac{1240}{330} = 3.76$ eV

This transition energy is in close agreement with the HOMO–LUMO energy gap (~4.08 eV) obtained from DFT calculations. The slight deviation is expected due to: Solvent effects, Vibronic transitions and Limitations of Koopmans' approximation. The absorption at 330 nm strongly suggests the presence of intramolecular charge transfer (ICT) within the molecule. This occurs when: The HOMO is localized over electron-rich (donor) regions, and the LUMO is localized over electron-deficient (acceptor) regions. Upon excitation, electron density shifts from donor to acceptor sites, leading to stabilization of the excited state and a red-shift in the absorption band. This behavior is consistent with: MEP analysis, showing charge-separated regions, Fukui functions, indicating reactive donor/acceptor sites and NBO analysis, revealing strong donor → acceptor interactions

3.3 Fukui Function Analysis

To gain deeper insight into local reactivity, Fukui functions were calculated using the finite difference approach. The Fukui indices f^+, f^-, and f^0describe the susceptibility of atomic sites toward nucleophilic, electrophilic, and radical attacks, respectively. The f^+values indicate that certain carbon and heteroatom centers act as preferred sites for nucleophilic attack, consistent with the LUMO localization. Conversely, the f^-values highlight electron-rich regions, particularly around heteroatoms, as favorable sites for electrophilic attack. The dual descriptor further confirms these observations by clearly distinguishing regions of electron donation and acceptance. The consistency between Fukui function results and MEP analysis demonstrates that the reactive sites identified are robust and reliable. Moreover, these findings complement the HOMO–LUMO analysis, where the spatial distribution of orbitals aligns with the predicted reactive centers. [38-43]

3.4 Natural Bond Orbital (NBO) Analysis

Natural Bond Orbital (NBO) analysis was performed to investigate intramolecular charge transfer and electron delocalization effects. The second-order perturbation theory analysis reveals significant donor–

acceptor interactions, particularly involving lone pair (LP) electrons of heteroatoms and antibonding orbitals (σ* and π*). Strong stabilization energies associated with interactions such as LP(N/O) → π*(C=C) and LP(N/O) → σ*(C–X) indicate pronounced electron delocalization within the molecular framework. These interactions contribute to the overall stabilization of the molecule and play a crucial role in determining its electronic properties. The presence of extensive conjugation and charge delocalization observed in the NBO analysis is in excellent agreement with the moderate HOMO–LUMO gap and the observed MEP charge distribution. Furthermore, the donor–acceptor interactions facilitate intramolecular charge transfer, which is essential for nonlinear optical (NLO) properties and biological activity. [38-43]

3.5 FT–IR Spectroscopic Analysis

The FT–IR spectrum of the synthesized compound was recorded in the range **4000–400 cm⁻¹** and provides important information regarding the functional groups present in the molecular framework. **Figure 6.**

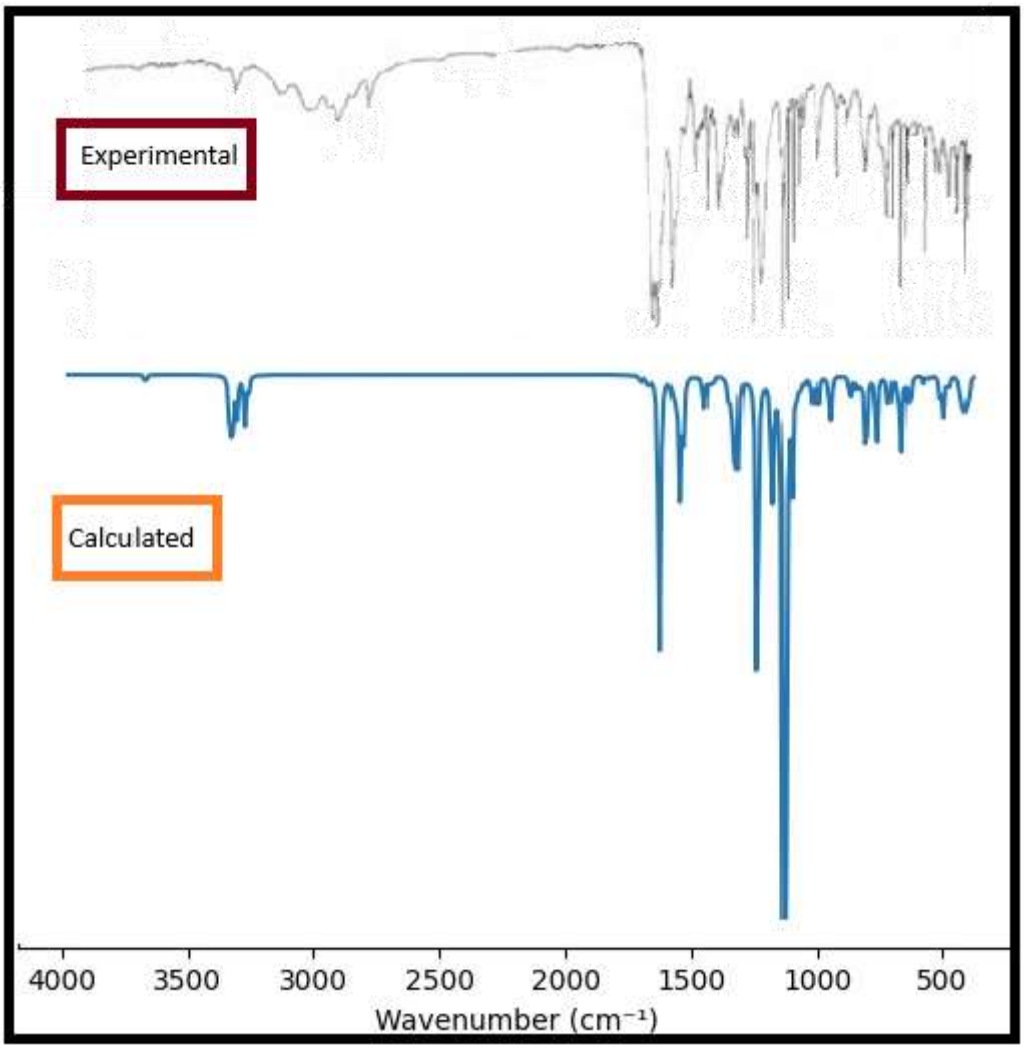

Figure 6. The experimental and theoretical FT–IR spectrum of Quinoxaline Derivative.

The observed vibrational bands confirm the successful formation of the target compound and are in good agreement with the proposed structure. The FT–IR spectrum of the synthesized compound, recorded in

the range 4000–400 cm^{-1}, exhibits characteristic absorption bands corresponding to key functional groups. The strong band observed at ~1560 cm^{-1} is attributed to C=N stretching vibration, while bands in the region 1470–1490 cm^{-1} correspond to aromatic C=C stretching. The presence of bands around 1200 cm^{-1} confirms C–N stretching vibrations, and the intense peak near 1100 cm^{-1} is assigned to C–O/C–N stretching modes. Additional bands in the fingerprint region further support the structural framework of the molecule. The observed spectral features are in good agreement with theoretical predictions, confirming the successful synthesis and structural integrity of the compound.

3.6 ^{1}H NMR Spectral Analysis (Experimental)

The ^{1}H NMR spectrum of the compound exhibits a singlet at δ 11.50 ppm corresponding to the amide (–CONH) proton, indicating strong deshielding due to the adjacent carbonyl group and possible hydrogen bonding. **Figure 7.** A singlet at δ 8.65 ppm is assigned to the azomethine (–CH=N–) proton, confirming the formation of the imine linkage. The aromatic protons appear as a multiplet in the region δ 7.13–8.54 ppm, integrating for ten protons, consistent with the presence of substituted aromatic rings. A singlet at δ 5.50 ppm integrating for two protons is attributed to the methylene (–OCH_2–) group. These spectral features are in excellent agreement with the proposed structure and theoretical calculations. Detailed Assignment and Interpretation; Amide Proton (–CONH) δ = 11.50 ppm (singlet, 1H) Assigned to amide NH proton. Highly downfield shifted due to: Strong deshielding by adjacent carbonyl (C=O) Possible intramolecular hydrogen bonding. The singlet nature indicates no coupling, typical for exchangeable NH protons. Imine Proton (–N=CH) δ = 8.65 ppm (singlet, 1H) Assigned to azomethine (imine) proton Appears downfield due to: Electron-withdrawing nitrogen Participation in conjugation with aromatic ring. The singlet confirms absence of neighboring protons. Aromatic Protons (Ar–H) δ = 7.13–8.54 ppm (multiplet, 10H) Corresponds to protons of two aromatic rings Multiplet pattern arises due to: Complex coupling (ortho, meta and para interactions) Different substitution environments The broad range indicates electron-donating and withdrawing substituent effects. Methylenic Protons (–OCH_2–) δ = 5.50 ppm (singlet, 2H) Assigned to methylene group attached to oxygen (–OCH_2–) Downfield shift due to: Electronegative oxygen atom Conjugation with adjacent functional groups. Singlet indicates no neighboring protons for coupling Structural Correlation. The observed proton signals strongly support the proposed molecular structure: Presence of amide group → confirmed by NH at 11.50 ppm Presence of imine linkage (–CH=N–) → confirmed by signal at 8.65 ppm Two aromatic rings → supported by 10H multiplet Ether/methylene linkage (–OCH_2–) → confirmed at 5.50 ppm

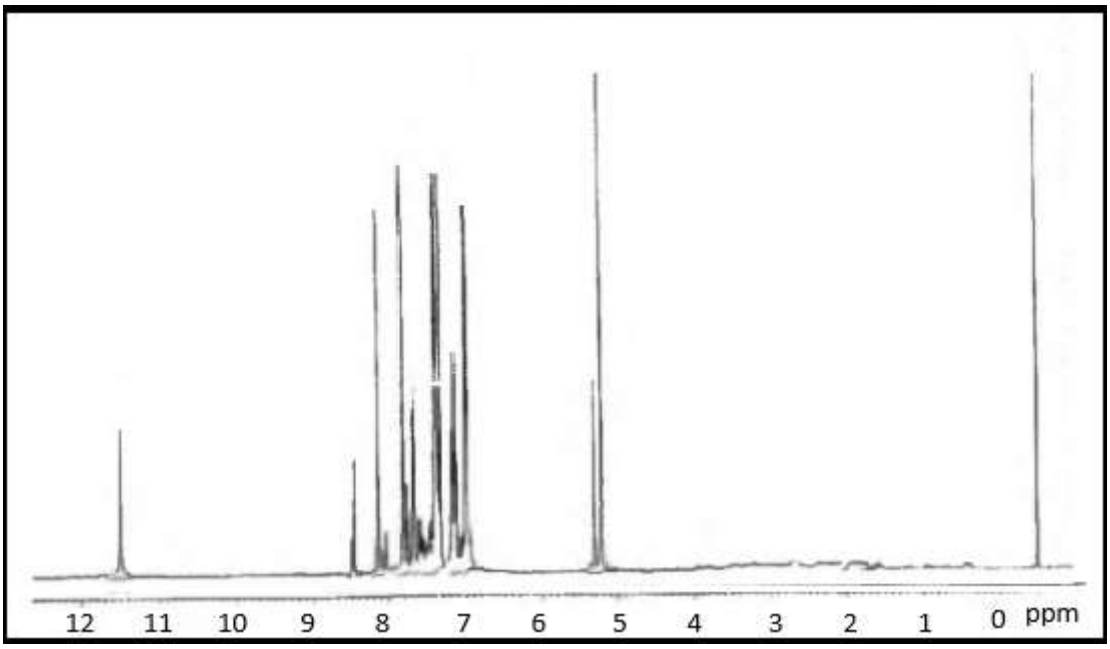

Figure 7. The ^{1}NMR spectrum of Quinoxaline Derivative.

Conclusion

In this study, a structurally significant heterocyclic compound was successfully investigated using a combination of experimental spectroscopic techniques and theoretical DFT calculations. The FT–IR spectrum confirmed the presence of key functional groups, including C=N, C=O, and C–N moieties, validating the proposed molecular framework. The ^{1}H NMR spectral data further supported the structure through the identification of characteristic signals corresponding to amide (–CONH), azomethine (–CH=N–), aromatic, and methylene protons. The UV–Visible spectrum exhibited a prominent absorption maximum at 330 nm, attributed to $\pi \rightarrow \pi^*$ electronic transitions within the conjugated system, indicating significant electron delocalization and intramolecular charge transfer (ICT). These experimental observations were found to be in good agreement with the theoretical HOMO–LUMO energy gap, suggesting moderate stability and appreciable reactivity of the molecule. The DFT-based global reactivity descriptors revealed that the compound possesses moderate chemical hardness and notable electrophilic character, making it a potential candidate for charge-transfer interactions. Furthermore, MEP analysis identified distinct electron-rich and electron-deficient regions, while Fukui function analysis provided insight into the preferred reactive sites for electrophilic and nucleophilic attacks. NBO analysis confirmed strong donor–acceptor interactions and extensive electron delocalization, contributing to the overall stabilization of the molecular system. Overall, the excellent correlation between experimental and theoretical results confirms the structural integrity and electronic properties of the compound. The presence of conjugation, heteroatoms, and charge-transfer characteristics suggests that the molecule holds promise for applications in materials chemistry, nonlinear optics, and potential biological activity. This comprehensive study demonstrates the effectiveness of combining spectroscopic techniques with DFT calculations for the detailed characterization of a novel quinoxaline derivative compound.

References

1. Porter, A. E. In Comprehensive Heterocyclic Chemistry; Katritzky, A. R., Rees, C. W., Eds; 1984; Vol. 3, part 2B, p 157.
2. Sato, N. In Comprehensive Heterocyclic Chemistry II; Katritzky, A. R., Rees, C. W., Scriven, E. F. V., Eds; Pergamon: Oxford, 1996; Vol. 6, p 233.
3. Seitz, L. E.; Suling, W. J.; Reynolds, R. C. J. Med. Chem. 2002, 45, 5604.
4. Gazit, A.; App, H.; McMahon, G.; Chen, A.; Levitzki, A.; Bohmer, F. D. J. Med. Chem. 1996, 39, 2170.
5. Monge, A.; Palop, J. A.; Del Castillo, J. C.; Caldero, J. M.; Roca, J.; Romero, G.; Del Rio, J.; Lasheras, B. J. Med. Chem. 1993, 36, 2745.
6. Toshima, K.; Takano, R.; Ozawa, T.; Matsumara, S. Chem. Commun. 2002, 212.
7. Wu, Z.; Ede, N. J. Tetrahedron Lett. 2001, 42, 8115.
8. Lee, J.; Murray, W. V.; Rivero, R. A. J. Org. Chem. 1997, 62, 3874.
9. Holland, R. J.; Hardcastle, I. R.; Jarman, M. Tetrahedron Lett. 2002, 43, 6435.
10. Krchnak, V.; Smith, J.; Vagner, J. Tetrahedron Lett. 2000, 41, 2835.
11. Uxey, T.; Tempest, P.; Hulme, C. Tetrahedron Lett. 2002, 43, 1637.
12. Zaragoza, F.; Stephensen, H. J. Org. Chem. 1999, 64, 2555.
13. Sonawane, N. D.; Rangnekar, D. W. J. Heterocycl. Chem. 2002, 39, 303.
14. Katoh, A.; Yoshida, T.; Ohkando, J. Heterocycles 2000, 52, 911.
15. Dailey, S.; Feast, J. W.; Peace, R. J.; Sage, I. C.; Till, S.; Wood, E. L. J. Mater. Chem. 2001, 11, 2238.
16. O'Brien, D.; Weaver, M. S.; Lidzey, D. G.; Bradley, D. D. C. Appl. Phys. Lett. 1996, 69, 881.
17. Mizuno, T.; Wei, W.-H.; Eller, L. R.; Sessler, J. L. J. Am. Chem. Soc. 2002, 124, 1134.
18. Elwahy, A. H. M. Tetrahedron 2000, 56, 897.
19. Crossley, J. C.; Johnston, L. A. Chem. Commun. 2002, 1122.
20. Antoniotti, S.; Dunach, E. Tetrahedron Lett. 2002, 43, 3971.
21. Petukhov, P. A.; Tkachev, A. V. Tetrahedron 1997, 53, 9761.
22. Juncai, F.; Yang, L.; Qinghua, M.; Bin. L. Synth. Commun. 1998, 28, 193.
23. Raw, S. A.; Wilfred, C. D.; Taylor, R. J. K. Chem. Commun. 2003, 2286.
24. Kaupp, G.; Naimi-Jamal, M. R. Eur. J. Org. Chem. 2002, 1368.
25. Chen, P.; Barrish, J. C.; Iwanowicz, E.; Lin, J.; Bednarz, M. S.; Chen, B.-C. Tetrahedron Lett. 2001, 42, 4293.
26. Soderberg, B. C. G.; Wallace, J. M.; Tamariz, J. Org. Lett. 2002, 4, 1339.
27. Suginome, M.; Collet, S.; Ito, Y. Org. Lett. 2002, 4, 351.
28. Mukhopadhyay, R.; Kundu, N. G. Tetrahedron Lett. 2000, 41, 9927.
29. Bunce, R. A.; Herron, D. M.; Ackerman, M. L. J. Org. Chem. 2000, 65, 2847.
30. Banik, B. K.; Banik, I.; Hackfeld, L.; Becker, F. F. Heterocycles 2002, 56, 467.
31. Goswami, S.; Adak, A. K. Chem. Lett. 2003, 32, 678.
32. Koopmans, T. Über die Zuordnung von Wellenfunktionen und Eigenwerten zu den einzelnen Elektronen eines Atoms. *Physica* 1934, *1*, 104–113.
33. Geerlings, P.; De Proft, F.; Langenaeker, W. *Chem. Rev.* 2003, *103*, 1793–1874.
34. Fukui, K. *Science* 1982, *218*, 747–754.
35. Becke, A. D. *J. Chem. Phys.* 1993, *98*, 5648–5652.
36. Lee, C.; Yang, W.; Parr, R. G. *Phys. Rev. B* 1988, *37*, 785–789.

37. Frisch, M. J.; Trucks, G. W.; Schlegel, H. B.; et al. Gaussian 09, Revision D.01; Gaussian, Inc.: Wallingford CT, 2009.
38. Reed, A. E.; Weinhold, F. Dimer. *J. Chem. Phys.* 1985, *83*, 1736–1740.
39. Politzer, P.; Murray, J. S. *Theor. Chem. Acc.* 2002, *108*, 134–142.
40. Domingo, L. R. *J. Org. Chem.* 2002, *67*, 5122–5125.
41. Chattaraj, P. K.; Sarkar, U.; Roy, D. R. *Chem. Rev.* 2006, *106*, 2065–2091.
42. Parr, R. G.; Szentpály, L. v.; Liu, S. *J. Am. Chem. Soc.* 1999, *121*, 1922–1924.
43. Lu, T.; Chen, F. *J. Comput. Chem.* 2012, *33*, 580–592.